Nuclear Instruments and Methods in Physics Research B 96 (1995) 508–516

NIM B
Beam Interactions with Materials & Atoms

ELSEVIER

Computational models for multiphonon scattering from surfaces: applications to He scattering from insulators

Srilal M. Weera, J.R. Manson *

Department of Physics and Astronomy, Clemson University, Clemson, SC 29634, USA

Abstract

We consider the inelastic interaction of a neutral atomic projectile scattering from a solid surface. Several computational models are developed to analyze the diffuse multiphonon component in the scattered intensity. Through extensive numerical calculations we determine the validity ranges of these approximations. Comparisons with experimental data for He scattering from LiF(001) and KCN(001) provide examples of the applicability of these theoretical approximations.

1. Introduction

Atom–surface scattering at thermal energies has proven to be an extremely sensitive and useful method of surface analysis [1,2]. The multiphonon contribution to the scattering process is observed as a diffuse inelastic background upon which the elastic and single phonon peaks appear. We present in this paper several computational models developed to describe the multiphonon intensity. One important reason for studying the multiphonon contribution is to better understand how to subtract the diffuse inelastic background in order to obtain accurate elastic and single phonon intensities. The single phonon intensity depends very strongly on the details of the phonon spectral density, whereas the multiphonon contribution does not since exchange of several quanta of energy tends to average over details of the phonon spectral density. This insensitivity to details in the phonon dynamics means that, through the use of simple phonon models, the information on the atom–surface interaction potential (i.e., the form factor for inelastic scattering), can be extracted.

The theory described here is quantum mechanical, and thus capable of treating the case of scattering of small mass particles such as He. We also consider the semiclassical limit which is valid for higher surface temperatures, higher incident energy particles and larger mass particles. Through extensive computational work we determine the ranges of validity for the approximations developed. We make comparisons with recent data for the scattering of He by LiF(001) which is a highly ordered surface, and by KCN(001) which appears to have significant disorder. In both cases good agreement is obtained between theory and the measured diffuse inelastic background.

2. Theory

We briefly review the important features of the quantum mechanical theory that has been developed previously [3,4] to analyze the multiphonon background. The interaction between the atomic projectile and the surface can be described by a Hamiltonian of the form

$$H = H^{\mathrm{p}} + H^{\mathrm{c}} + V, \tag{1}$$

where H^{p} is the Hamiltonian of the free particle, H^{c} is the Hamiltonian of the unperturbed crystal which includes the phonon vibrational states and V is the interaction coupling the projectile and crystal.

The experimentally measured quantity is the three-dimensional differential reflection coefficient, $\mathrm{d}R/\mathrm{d}\Omega_{\mathrm{f}}\,\mathrm{d}E_{\mathrm{f}}$ which gives the fraction of the incident particles that are scattered into final solid angle $\mathrm{d}\Omega_{\mathrm{f}}$ and energy interval $\mathrm{d}E_{\mathrm{f}}$. It is related to the transition rate for scattering $w(k_{\mathrm{f}}, k_{\mathrm{i}})$ from projectile state k_{i} to state k_{f}, upon dividing by the incident flux and multiplying by the density of available final particle states:

$$\frac{\mathrm{d}R}{\mathrm{d}\Omega_{\mathrm{f}}\mathrm{d}E_{\mathrm{f}}} = \frac{m^2 |k_{\mathrm{f}}|}{(2\pi\hbar)^3 k_{\mathrm{i}z}} w(k_{\mathrm{f}}, k_{\mathrm{i}}). \tag{2}$$

The standard approach is to start with the quantum mechanical probability density for the projectile to gain an amount of energy E, or to start from the generalized golden rule for the transition rate for scattering, which is given by

$$w(k_{\mathrm{f}}, k_{\mathrm{i}}) = \frac{2\pi}{\hbar} \langle\langle \sum_{n_t} |T_{\mathrm{fi}}|^2 \delta(\mathscr{E}_{\mathrm{f}} - \mathscr{E}_{\mathrm{i}}) \rangle\rangle, \tag{3}$$

* Corresponding author. e-mail: jmanson@phonon.phys.clemson.edu.

SSDI 0168-583X(95)00312-6

where T_{fi} is the transition matrix element, $\mathscr{E}_q$ denotes the energy of the total system (projectile plus crystal), the summation Σ_{n_t} is over the final vibrational states of the crystal and the double brackets $\langle\langle\rangle\rangle$ imply an average over the initial states of the crystal. The transition rate is proportional to the time derivative of the probability density, and both contain the same information. Using the interaction picture, the time dependence of operators is expressed in terms of the unperturbed crystal Hamiltonian:

$$\hat{T}(t) = \mathrm{e}^{\mathrm{i}H^{\mathrm{c}}t/\hbar}\hat{T}\,\mathrm{e}^{-\mathrm{i}H^{\mathrm{c}}t/\hbar}. \tag{4}$$

It has been demonstrated that within the approximations discussed below, a satisfactory starting point is to make the following simple and straightforward approximation to the matrix elements of the transition operator taken with respect to particle eigenstates:

$$T_{k_{\mathrm{f}},k_{\mathrm{i}}}(t) = \left(k_{\mathrm{f}}\,|\,\hat{T}(t)\,|\,k_{\mathrm{i}}\right) = \sum_l \mathrm{e}^{-\mathrm{i}k\cdot[r_l+u_l(t)]}\tau_{k_{\mathrm{f}},k_{\mathrm{i}}}, \tag{5}$$

where $k = k_{\mathrm{f}} - k_{\mathrm{i}}$, r_l is the equilibrium position vector of the lth unit cell and $u_l(t)$ is its vibrational displacement. The summation is over unit cells of the surface, i.e., the only dependence on the crystal displacements is in the phase arising from the optical path, then the transition rate resulting from Eq. (3) is

$$w(k_{\mathrm{f}},\,k_{\mathrm{i}}) = \frac{N}{\hbar^2}\int_{-\infty}^{+\infty}\mathrm{d}t\;\mathrm{e}^{-\mathrm{i}Et/\hbar}\,|\,\tau_{\mathrm{fi}}\,|^2\sum_l \mathrm{e}^{\mathrm{i}K\cdot R_l} \times \mathrm{e}^{-2W(k)}\,\mathrm{e}^{\langle\langle k\cdot u_0(0)k\cdot u_l(t)\rangle\rangle} \tag{6}$$

where K and R_l are the component of k and r_l parallel to the surface, $E = E_{\mathrm{f}} - E_{\mathrm{i}}$ is the difference between the final and initial particle energy (i.e., the energy gain of the particle), N is the number of surface unit cells and τ_{fi} is the form factor of a unit cell. It can be shown that τ_{fi} is the contribution from a unit cell of the off-energy-shell transition matrix [4]. The important underlying assumption here is the quick collision approximation, which implies that for a fast incident particle the scattering time is short compared to a phonon vibrational period. Note that the quick collision approximation does not imply a hard wall collision, it implies simply that the time during which the particle is near the surface is short compared to that of the periods of the phonons which will be exchanged during the collision. This is a valid assumption for the low frequency and long wavelength phonons that mainly comprise the multiphonon part of the spectrum. The displacement correlation function appearing in the exponential of Eq. (6) is the time dependent correlation function of an element of the surface and can be expressed in terms of the normal modes of the crystal. The Debye–Waller exponent can be expressed in the standard form involving the mean square displacement:

$$2W(R,\,k) = \langle\langle\left[k\cdot u_l(R,\,t)\right]^2\rangle\rangle. \tag{7}$$

The Debye–Waller factor, $\exp(-2W)$, is seen to multiply all contributions to the scattering, either elastic or inelastic. Formally, as indicated by its dependence on the mean square vibrational amplitude as shown in Eq. (7), it can be explained in terms of multiple scattering of virtual phonons [9]. It can also be described as a consequence of unitarity, or the conservation of the number of scattered particles. As more and more inelastic channels open up with increasing temperature and incident energy, the existing channels must decrease in intensity in order to conserve the total number of particles scattered into all possible final states.

Eq. (6) provides the total scattered intensity, from which zero and single phonon components need to be subtracted to obtain the multiphonon contribution. All numbers of multiple phonon exchange are contained in the exponentiated displacement correlation function. The method to obtain different phonon contributions is to expand the exponential of the displacement correlation function in Eq. (6). Upon expanding the exponential to zero or first order in the displacement correlation function, the elastic and single phonon contributions are obtained. The remaining terms of the expansion is the multiphonon part.

2.1. Exact method

To facilitate numerical computation, various approximations to the theory need to be considered. Starting with the exact form of the theory, the multiphonon contribution according to Eq. (6) is

$$\frac{\mathrm{d}R}{\mathrm{d}\Omega_{\mathrm{f}}\,\mathrm{d}E_{\mathrm{f}}} = \frac{m^2\,|\,k_{\mathrm{f}}\,|}{8\pi^3\hbar^5 k_{\mathrm{i}z}}\,|\,\tau_{\mathrm{fi}}\,|^2\,\mathrm{e}^{-2W}\int_{-\infty}^{+\infty}\mathrm{d}t\;\mathrm{e}^{-\mathrm{i}Et/\hbar}\sum_l \mathrm{e}^{-\mathrm{i}K\cdot R_l} \times\left[\exp\left(\langle\langle k\cdot u_0(0)k\cdot u_l(t)\rangle\rangle\right) - \left(\langle\langle k\cdot u_0(0)k\cdot u_l(t)\rangle\rangle\right) - 1\right]. \tag{8}$$

The displacement correlation function appearing in the above equation can be evaluated assuming a three-dimensional isotropic Debye model. The frequency distribution in this case, is

$$\rho(\omega) = 3\omega^2/\omega_{\mathrm{D}}^3, \tag{9}$$

where ω_{D} is the Debye frequency of the crystal.

The resulting expression for the displacement correlation function is

$$\langle\langle n_i\,|\,k\cdot u_0(0)k\cdot u_l(t)\,|\,n_i\rangle\rangle = \frac{3\hbar\,|\,k\,|^2}{2M\omega_{\mathrm{D}}}\int_0^1\frac{\mathrm{d}\omega}{\omega}\frac{\sin\left(\dfrac{\omega R_l}{v}\right)}{\left(\dfrac{\omega R_l}{v}\right)} \times\left\{\left[2n(\omega)+1\right]\cos(\omega t) - \mathrm{i}\sin(\omega t)\right\}, \tag{10}$$

where $n(\omega)$ is the Bose–Einstein function.

Eq. (8) will be referred to as the Exact Discrete Method, since it contains a summation over the lattice sites. This formula could be used to analyze surfaces containing discrete scattering centers. We have applied it to the case of alkali halides, and were able to obtain good agreement with the data. But for metals like copper, which has a free electronic distribution, a different formula is required. In this case, the sum over lattice sites appearing in Eq. (8) needs to be replaced by an integral in the continuum limit [10].

For the form factor $|\tau_{fi}|^2$ appearing in Eq. (8), we have adopted expressions obtained from the distorted wave Born approximation which have proven to be very useful in treatments of single phonon scattering [11–13]. The form factor was expressed as a product of a Mott–Jackson matrix element for perpendicular motion and a cut-off factor for parallel motion:

$$|\tau_{fi}|^2 = e^{-K^2/Q_c^2} v_{M-J}^2(k_{fz}, k_{iz}). \tag{11}$$

The Mott–Jackson factor v_{M-J} is the matrix element of the one-dimensional potential $v(z) = \exp\{-\beta z\}$ taken with respect to its own distorted eigen-states. The cut-off factor in Eq. (11) has a Gaussian form in K, and the Mott–Jackson factor behaves roughly as an exponential decay in the normal momentum difference $|k_{fz}| - |k_{iz}|$ when this quantity is sufficiently large.

2.2. FT method

We can simplify the expressions derived in the above section in the first-order semiclassical limit. Assuming only the long wavelength or small frequency phonons contribute strongly to the multiphonon intensity, the displacement correlation function can be simplified in terms of a small wave vector expansion. The details of this procedure can be found in Ref. [4]. A simplified result is obtained for the case of a Bravais unit cell. The differential reflection coefficient now assumes the following form

$$\frac{dR}{d\Omega_f\, dE_f} = \frac{m^2 |k_f|}{8\pi^3 \hbar^5 k_{iz}} |\tau_{fi}|^2 e^{-2W(k)} S(K, E) I(K, E). \tag{12}$$

This is the product of a form factor $|\tau_{fi}|^2$, a Debye–Waller factor, a structure factor $S(K, E)$ due to periodicity of the surface, and an energy exchange factor $I(K, E)$. The specific expressions for these quantities are given by

$$S(K, E) = \sum_l e^{-iK\cdot R_l} e^{-F_l}, \tag{13}$$

with

$$F_l = \sum_{\alpha,\alpha'=1}^{3} k_\alpha k_{\alpha'} \sum_{Q,\nu} \frac{\hbar (Q\cdot R_l)^2}{2NM\omega_\nu(Q)} e_\alpha\left(\frac{Q}{\nu}\right) e_{\alpha'}^*\left(\frac{Q}{\nu}\right) \times [2n(\omega_\nu(Q)) + 1] \tag{14}$$

and

$$I(K, E) = \int_{-\infty}^{+\infty} dt\, e^{-iEt/\hbar}\left(e^{Q(t)} - Q(t) - 1\right), \tag{15}$$

with

$$Q(t) = \sum_{\alpha,\alpha'=1}^{3} k_\alpha k_{\alpha'} \sum_{Q,\nu} \frac{\hbar}{2NM\omega_\nu(Q)} e_\alpha\left(\frac{Q}{\nu}\right) e_{\alpha'}\left(\frac{Q}{\nu}\right) \times \left([2n(\omega_\nu(Q)) + 1]\cos(\omega_\nu(Q)t) - i \times \sin(\omega_\nu(Q)t)\right), \tag{16}$$

where M is the mass of the surface atom, Q is the parallel wave vector of the phonon mode, ν is a discrete quantum number for surface modes and continuous for bulk modes, $e_\alpha\left(\frac{Q}{\nu}\right)$ is the polarization vector of the (Q, ν) mode and $\omega_\nu(Q)$ is the mode frequency. In the limit $t \to 0$, $Q(t)$ is just the Debye–Waller exponent of Eq. (7), and F_l is a closely related sum in which the summand is weighted by the square of the parallel momentum. In Eq. (15) $I(K, E)$ is the multiphonon contribution after subtracting off the elastic and single phonon parts.

To evaluate the above formulas, a frequency distribution is required. This has been done by assuming a 3D Debye distribution. Eq. (16) now simplifies to

$$Q(t) = \frac{3\hbar |k|^2}{2M\omega_D}\left[\int_0^1 d\omega\, \omega \cos(\omega t)\left(\frac{2}{\exp\left(\frac{\hbar\omega_D\omega}{k_B T}\right) - 1} + 1\right) - i(\sin t - t\cos t)/t^2\right]. \tag{17}$$

The single phonon part can be calculated by expanding the exponential of the displacement correlation function in Eq. (6) to the first order. The resultant expression in the Debye model is

$$\frac{dR}{d\Omega_f\, dE_f}^{1\text{phonon}} = \frac{m^2 |k_f|}{8\pi^3 \hbar^5 k_{iz}} e^{-2W(k)} |\tau_{fi}|^2 \frac{6\pi\hbar\omega |k|^2}{2M\omega_D} \times \left(\frac{1}{\exp\left(\frac{\hbar\omega_D\omega}{k_B T}\right) - 1}\right), \tag{18}$$

where T is the surface temperature of the crystal. The above expression is applicable in the range of $|\omega| \le \omega_D$. Since the above formulas are applicable throughout the full temperature range this method will be called the FT method.

2.3. HT method

Although the FT method described above works from low to high temperatures, it is still possible to obtain a

simpler semiclassical formula at high temperatures. This is carried out by expanding $n(\omega)$ for large T and simultaneously expanding the imaginary part of $Q(t)$ in small t. We have evaluated these expressions in the Debye model to enable comparison with the experiment. The explicit forms at high temperatures are

$$S(K, E) = \sum_l e^{-iK\cdot R_l} \exp\left[\frac{-\omega_0 k_B T R_l^2}{2\hbar v_R^2}\right], \tag{19}$$

and

$$I(K, E) = \int_{-\infty}^{+\infty} dt\, e^{-i(E/\hbar+\omega_0)t}[\exp(Q(t)) - Q(t) - 1], \tag{20}$$

where v_R is a characteristic velocity or weighted average of surface phonon velocities parallel to the surface and $Q(t)$ takes on the simpler form $Q(t) = 2W(k)\sin(\omega_D t)/\omega_D t$. In the HT method, the Debye–Waller exponent takes the familiar form

$$2W(k) = \frac{3|k|^2 k_B T}{M\omega_D^2}, \tag{21}$$

and the energy shift is given by

$$\hbar\omega_0 = \hbar^2 k^2/2M. \tag{22}$$

This approximation, consisting of Eqs. (19) and (20) and applicable at high temperatures, will be called the HT method. Note that to obtain the multiphonon contribution, the zero and first order terms must be subtracted as in Eq. (15) above.

Eqs. (15) through (22) have been used in the calculations to compare with the data. Before applying these formulas, however, it is necessary to know the conditions under which they are applicable. To determine these conditions, we have carried out an extensive study for a wide range of parameters. Our results show that the high temperature approximation to the first-order semiclassical limit is applicable when the temperature is above half the Debye temperature of the crystal [14].

The energy shift has its origins in the zero-point motion and is the result of recoil motion of the crystal. It occurs in the above analysis due to a further approximation of replacing the $\sin(\omega_\nu(Q)t)$ function in Eq. (16) by its argument. This approximation is not necessary, but it is quite accurate in the extreme semiclassical region of large incident energies where $\hbar\omega_0$ can be interpreted as the energy loss to the surface of an energetic incident particle when $\hbar\omega_0 \ll E_i$. In general, and particularly for He scattering, $\hbar\omega_0$ is not small compared to E_i and in these circumstances the average energy loss must be calculated as an integral over $dR/d\Omega_f\, dE_f$ weighted by the energy exchange to the particle, $E = E_f - E_i$.

It should be noted that the prefactor $|k_f|/k_{iz}$ occurring in Eq. (12) is suitable for the standard experimental configuration. This refers to the case when the detector acceptance angle covers the entire illuminated spot made by the incident beam. For other configurations different prefactors would apply. Our data analysis has shown the importance of using the correct prefactor applicable for the specific configuration of the scattering apparatus.

2.4. CL method

We now consider the classical limit, which we denote by the CL method. This occurs under conditions when the temperature and incident energy are high. Under such near-classical and classical scattering conditions the Debye–Waller factor is so small that elastic and single phonon peaks are completely suppressed, and only multiphonon exchanges occur. It is of interest to consider the present theory in this limit as it leads to closed form expressions for the scattering intensities, and provides specific criteria for the validity of the classical limit. We consider the case of scattering of a point projectile with a lattice of discrete atomic centers. Under these conditions, the energy exchange factor appearing in Eq. (12) can be evaluated using the method of steepest descents [3], upon expanding the $Q(t)$ of Eq. (16) to order t^2. The final result is

$$\frac{dR}{d\Omega_f\, dE_f} = \frac{m^2|k_f|}{8\pi^3\hbar^5 k_{iz}}|\tau_{fi}|^2\left(\frac{\hbar\pi}{\omega_0 k_B T}\right)^{1/2} \times \exp\left\{-\frac{(E+\hbar\omega_0)^2}{4k_B T\hbar\omega_0}\right\}. \tag{23}$$

The structure factor of Eq. (13) is equal to one, implying that the structure effects are negligible in the classical limit. The Debye–Waller factor no longer appears explicitly in this expression because it has been canceled by a term arising from the energy exchange factor.

The steepest descent evaluation of Eq. (12) implies a criterion for the validity of the semiclassical result, which is

$$2W(k)/6 \gg 1. \tag{24}$$

This is a very stringent criterion since $2W$ is approximately equal to the average number of phonons exchanged in a collision. This condition is rarely satisfied in helium scattering, but often achieved with large mass atomic probes such as Kr, Xe and Ar.

It is pertinent to mention here that the theory provides another classical limit that is applicable for continuum surfaces. Eq. (23) is the classical limit for a point particle scattering from a lattice of scattering centers in the limit in which the projectile scatters from a single surface atom. There is a second classical limit for the case of an incident projectile which interacts with many surface atoms, and the surface can be treated as a continuum. This is the limit that should be applicable for example in the completely classical case of a projectile that is large compared to the

interatomic lattice spacing. In this limit, the structure factor in Eq. (13) does not approach a constant, rather it has a Gaussian behavior in parallel momentum. This expression is obtained by replacing the summation over lattice sites in Eq. (13) by an integral. The final result is a differential reflection coefficient of the following form:

$$\frac{\mathrm{d}R}{\mathrm{d}\Omega_\mathrm{f}\,\mathrm{d}E_\mathrm{f}} = \frac{m^2|k_\mathrm{f}|}{4\pi^3\hbar^5 k_{\mathrm{i}z} S_{\mathrm{u.c.}}} |\tau_{\mathrm{fi}}|^2 v_\mathrm{R}^2 \left(\frac{\hbar\pi}{\omega_0 k_\mathrm{B} T}\right)^{3/2} \times \exp\left\{-\frac{(E+\hbar\omega_0)^2 + 2\hbar^2 v_\mathrm{R}^2 K^2}{4k_\mathrm{B} T\hbar\omega_0}\right\}, \tag{25}$$

where v_R is the same characteristic velocity of Eq. (19). There is a clear difference between the two classical limits of Eqs. (23) and (25). In the latter, the temperature dependence of the peak in the inelastic intensity varies as $1/T^{3/2}$ as opposed to $1/T^{1/2}$, and there is the extra Gaussian behavior in parallel momentum exchange.

3. Validity ranges of the approximations

The primary purpose of deriving these approximations was to develop computational tools that could be used to analyze the experimental data. Hence, it is important to know the applicable ranges of validity for the approximations. Although the HT method is generally applicable at high temperatures and the CL method under classical conditions, a comprehensive study needs to be carried out to ascertain precisely what these conditions are. Each method needs to be tested under a variety of conditions and compared with the calculated results based on other methods. In our study the experimentally variable input parameters: i.e., the incident energy of the particle (E_i), mass of the particle (m), mass of the crystal atom (M) and the Debye temperature of the surface (Θ_D) were varied over a wide range. For each value of the variables listed above, the differential reflection coefficient (which is proportional to the measured intensity, I) vs the particle energy exchange, ΔE was plotted for a given final angle and for the entire range of the temperatures investigated. From the large number of plots thus generated, the peak height ($I_{\max}$), full-width-at-half-maximum (FWHM) and the Debye–Waller exponent ($2W$) at zero energy exchange ($\Delta E = 0$) were extracted. The same procedure was repeated for each run of the FT, HT and CL methods. Then, $I_{\max}$, FWHM and $2W$ were plotted against the range of temperatures for each value of the parameters. A sample plot is shown in Fig. 1, which illustrates the behavior of the HT and FT methods over the temperature range. The calculations were produced assuming He scattering from an NaCl(001) surface in the ⟨110⟩ direction.

In the bottom window the maximum of the scattered multiphonon intensity is plotted against temperature. At low temperatures, understandably the results based on the HT method are quite different from the FT calculations. This occurs since the underlying assumption for the HT approximation is that the temperatures should be sufficiently high. However, the HT method (dashed line) quickly approaches the FT method (solid line) as the temperature is raised. In the middle window, the FWHM is compared for the two methods under the same conditions. The top window shows the predicted behavior of the Debye–Waller exponent for the two approximations.

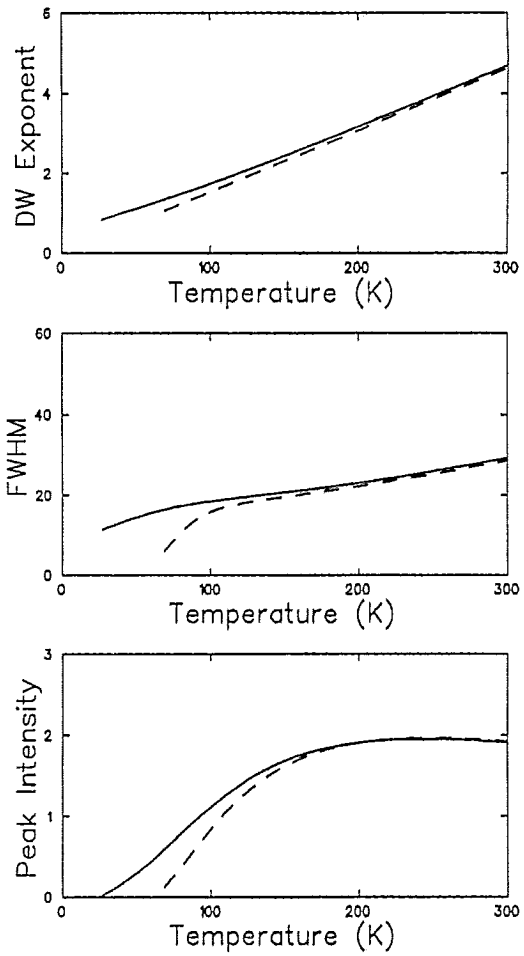

Fig. 1. A comparison of the peak intensity, FWHM and Debye–Waller exponent for FT and HT methods. The solid line is based on the FT method calculations while the dashed line shows the behavior of the HT method. The parameters used in the calculation were; $\theta_\mathrm{i} = 45°$, $k_\mathrm{i} = 9.2$ Å^{-1}, $\Theta_\mathrm{D} = 215$ K, $m = 40$ amu and $M = 35.5$ amu for He scattering from NaCl(001) ⟨110⟩.

3.1. HT method

Our intent in this study is to determine a criterion that could be used to predict the applicability of the approximation. For example, is it the magnitude of the Debye–Waller exponent (since it plays such a central role in atom–surface

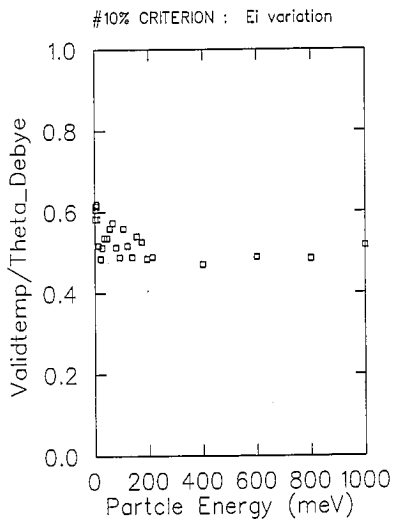

Fig. 2. Validtemp/Θ_D vs energy of the incident particle (E_i). The calculations were produced for a He/NaCl system at specular incidence. Assumed values for the Debye temperature and crystal mass were 215 K and 35.5 amu, respectively.

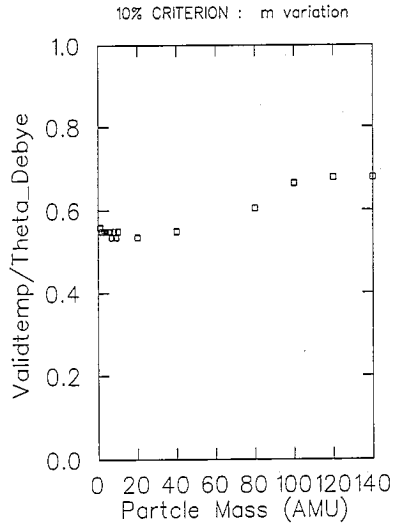

Fig. 3. Validtemp/Θ_D vs mass of the particle (m). The calculations were produced for a He/NaCl system with 44.23 meV particle energy at specular incidence. Assumed value for the Debye temperature was 215 K.

scattering) or is it the temperature of the crystal, that determines the applicability of the HT method. To examine this, we first need to specify a test under which the HT method is considered to be in agreement with the FT method. For this purpose, in the I vs ΔE plot, the point at which the two calculations based on FT and HT methods first agree within 10% of each other will be called the 10% criterion. (A similar criterion is defined for the FWHM vs ΔE plot.) Next, the temperature at which the 10% criterion is satisfied (validtemp) was noted. Then for every case studied validtemp/Θ_D was plotted against the whole range of parameter values for incident particle energy, particle mass and crystal mass. The results of this study are shown in Figs. 2 through 4.

These studies demonstrate that in the whole range of the parameters studied, the 10% criterion occurs approximately when $T/\Theta_D > 0.5$. As an empirical rule, when the crystal temperature is above half of the Debye temperature, the HT method can be assumed to be a good approximation for the FT method. The above result on the validity of the HT method is consistent with the applicability of the high temperature approximation for specific heat calculations of general materials where it is usually agreed that the high temperature approximation can be used for $T > \Theta_D/2$ [9].

3.2. CL method

The CL method is applicable for high incident energies and at high temperatures. Hence, the validity criterion for the CL method is different from that for the HT method. At low temperatures, the CL method results diverge from FT or HT methods. This is to be expected since the CL method is applicable only under classical conditions. As the temperature is considerably increased, however, the CL method fast approaches the FT method. The regime of validity of the CL method has been studied in detail in Ref. [14]. Suffice it to mention that the results of the study indicate that, if $2W(k) > 4$ over the entire range of ΔE for which there is appreciable inelastic intensity, then the CL method works quite well in predicting the form of the diffuse inelastic background. We have noticed that under most conditions it is adequate to test the value of $2W$ at

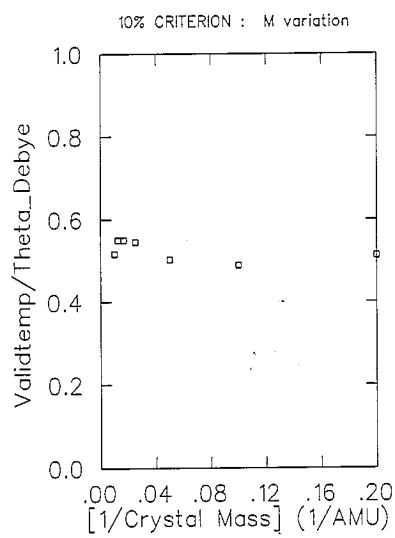

Fig. 4. Validtemp/Θ_D vs reciprocal of the crystal mass ($1/M$). The calculations were produced for a He/NaCl system with 44.23 meV particle energy at specular incidence. Assumed value for the Debye temperature was 215 K.

$\Delta E = 0$. However, when E_i or m/M is small, the value of $2W$ will vary strongly from small to large energy exchange, and its value at $\Delta E = 0$ may need to be substantially larger in order for the CL expression to be valid.

4. Applications in data analysis

Our first example is a comparison of the theory with the helium scattering data from LiF(100) ⟨110⟩. LiF was used in the first gas–crystal surface diffraction experiments conducted in the early 1930s by Stern and coworkers to investigate the wave nature of atoms. Scattering from well prepared LiF crystals produces strong diffraction patterns due to the highly corrugated nature of its surface. The ease of preparation of clean, ordered crystal samples by cleaving and then annealing in a vacuum makes LiF a good candidate for surface studies.

Figs. 5 and 6 present scattered intensity versus energy exchange for an incident beam of nearly 34 meV He atoms incident on a clean LiF(001) surface in the ⟨110⟩ direction for several surface temperatures. The He scattering apparatus has a fixed angle of 90° between the incident beam and the detector. The incident angles are 40° and 50°, respectively. These angles were chosen because they are not close to conditions for elastic diffraction. The jagged lines are the experimental time-of-flight data transformed into energy exchange spectra. The smooth lines are the theoretical calculations to compare with the estimated multiphonon backgrounds from the data curves. The temperatures are indicated on the graphs. Our calculations based on the semiclassical approximation of the theory predicts a rising multiphonon background with increasing temperature. The difference between the theory curve and the estimated multiphonon background from the experimental data curve at low temperatures can be attributed to the exchange due to bulk single phonons.

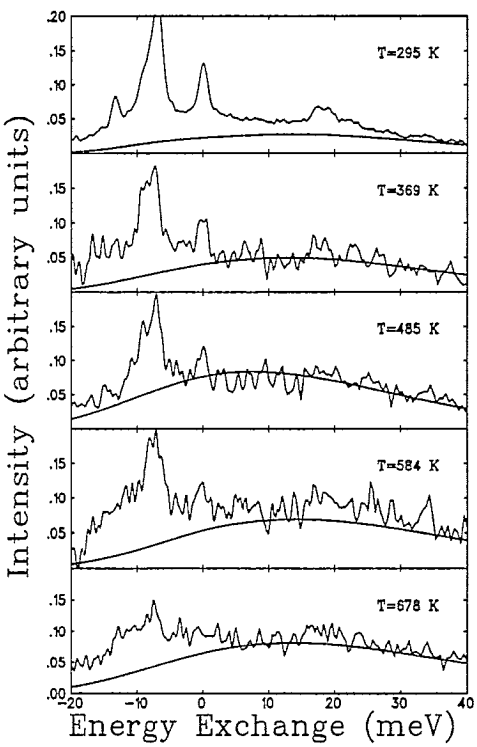

Fig. 5. The intensity vs energy exchange curves for He scattering from LiF(001) ⟨110⟩ at 40° incidence. The smooth lines are the theory curves to match with the data curves represented by jagged lines. The relevant parameters are; $E_i = 34$ meV, Debye temperature = 520 K, effective crystal mass = 12.97 amu, $\beta = 6.0$ Å^{-1} and $Q_c = 4.5$ Å^{-1}.

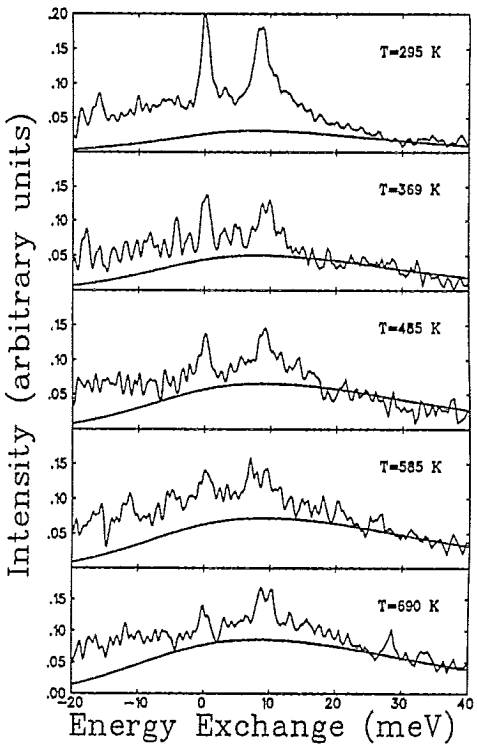

Fig. 6. Same as in Fig. 5 except at 50° incidence.

For the next example we present He scattering from KCN, which has a more disordered surface structure. Neutron inelastic scattering and Raman scattering made on KCN indicate that multiphonon effects play an important role [15]. A high degree of dynamic disorder of the CN^- ion and an unusually large Debye–Waller exponent have been observed in these studies. In the He scattering studies, reported here, these facts were confirmed for the case of surface scattering.

In our analysis of the KCN data we have noticed that at low temperatures there appears to be a substantial contribution to the inelastic intensity from the single phonons. For this surface the single phonon intensity would be expected to have a large incoherent contribution coming from the surface disorder. The incoherent distribution due

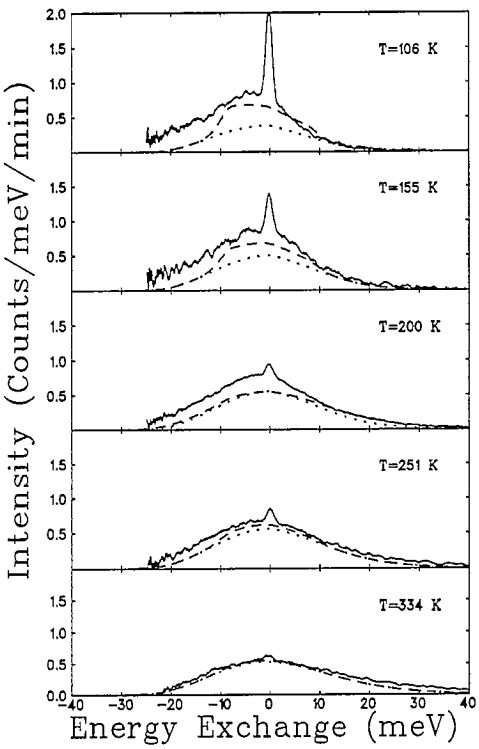

Fig. 7. The intensity vs energy exchange curves for He scattering from KCN at 45° incidence. The dotted lines indicate the calculated multiphonon backgrounds. The dashed lines are the theory curves (single plus multiphonon contributions) to match with the data curves represented by solid lines. The relevant parameters are; $E_i = 30$ meV, Debye temperature = 123 K, crystal mass = 65.10 amu, $\beta = 5.5$ Å^{-1} and $Q_c = 7.5$ Å^{-1}.

to small frequency vibrations is well represented by a Debye model. Consequently, we have calculated the Debye model single phonon contribution based on Eq. (18) and added it to the multiphonon part. Fig. 7 illustrates the comparisons made with the data for a range of temperatures. The dotted lines indicate the calculated multiphonon backgrounds whereas the solid lines represent the experimental data. The dashed lines are the theory curves for the total inelastic background (sum of single and multiphonon contributions). The temperatures are 334, 251, 200, 155 and 106 K. We have assumed a Debye temperature = 123 K, crystal mass = 65.10 amu, $\beta = 5.5$ Å^{-1} and $Q_c = 7.5$ Å^{-1}. Reasonably good agreement is obtained throughout the temperature range when the contribution due to single phonon exchange is included in the calculated intensities. At low temperatures, the difference in the two theoretical curves clearly indicates the magnitude and importance of the single phonon contributions. Furthermore, the shape of the single phonon contribution at low temperatures and in particular its sharp cut-off at the Debye frequency, gives a good estimate of the value that should be used for the surface Debye temperature.

5. Discussion

We have presented the essential features of the theory of multiphonon inelastic scattering of atomic projectiles by surfaces. The motion of the particle and the surface are treated quantum mechanically, and the transition to the correspondence limit of large numbers of quanta and to the semiclassical limit for particle motion are straightforward. This model should work well for multiphonon processes involving the exchange of low-energy, long-wavelength phonons. It is noted that the multiphonon background depends on the atom–surface interaction potential in the same way as the single phonon intensity. However, the single phonon intensity depends very strongly on the details of the phonon spectral density, whereas the multiphonon contribution does not since exchange of several quanta of energy tends to average over details of the phonon spectral density. This insensitivity to details in the phonon dynamics means that simple phonon models may be used to evaluate the multiphonon intensity. By subtracting off the multiphonon background from the total measured intensity, the single phonon peaks could now be accurately measured. Our calculations based on the theory show good agreement with the multiphonon inelastic background observed in helium scattering experiments. The theory illustrates the limits to which information on surface vibrational properties can be obtained from analysis of an experiment, without extensive knowledge of the specific and detailed nature of the He–surface interaction potential.

In our theoretical formulation of multiphonon scattering several approximations were developed which lead to straightforward and tractable numerical calculations. Three of the approximations were examined in detail, the first order semiclassical in both its full temperature and high temperature forms (FT and HT methods) and the classical limit (CL method). In the semiclassical limit the multiphonon background can be expressed as the product of a structure factor arising from the periodic nature of the surface, an energy exchange factor, a Debye–Waller factor for thermal attenuation and a form factor depending on the interaction potential. The structure factor approaches unity in the classical limit but in the quantum regime is peaked at momentum values corresponding to the two-dimensional surface diffraction peak positions, and for complicated surface unit cells can have additional structure between the diffraction peaks. The energy exchange function becomes a Gaussian-like function of the total energy exchanged between probe and surface with a shift $\hbar\omega_0$ in the direction of energy gain by the surface. The Debye–Waller factor is roughly equal to the average number of real or virtual phonons exchanged in the collision. The form factor was expressed as the product of a Mott–Jackson factor for perpendicular motion and a cutoff factor for parallel motion.

A large number of numerical calculations have been

carried out in order to establish the regimes of validity of each approximation. We find that over a very large range of initial parameters the HT approximation gives a good representation of the FT results as long as the surface temperature is greater than half of the Debye temperature of the surface. The regime of the classical approximation is somewhat more complicated. Formally, the closed form classical expressions of Eqs. (23) and (25) are valid only if $2W(k) \gg 6$. We found that the CL expression is a reasonably good representation of the multiphonon intensity if the Debye–Waller exponent $2W(k)$ is greater than 4 over the entire range of energy exchange for which the scattered intensity is non-negligible.

We have applied the semiclassical approximation of the theory to analyze the experimental data obtained for LiF (a highly ordered surface) and KCN (a more disordered surface). Our results indicate that over the temperature range considered, the first-order semiclassical approximation is a good representation of the theory. By subtracting off the estimated multiphonon background, the single phonon contribution could now be accurately evaluated. The ease of manipulation of the theory by varying just two parameters, the range parameter of the potential β and the cutoff parameter Q_c, is of practical use to the experimentalists. The parameter β enters through the assumed form of the repulsive part of the model potential, $\exp(-\beta z)$, where z is normal to the surface. A large value of β thus causes the potential to fall off faster, approaching the hard wall limit. On the other hand a small β indicates a softer potential that falls off gradually from the surface, which is more characteristic for metals. The cutoff momentum parameter, Q_c is contained in the term $\exp(-K^2/Q_c^2)$. Hence a small value of Q_c would limit the attainable K values in the momentum space, thereby introducing a cutoff factor. On the other hand, large values of Q_c render it possible to exchange large values of parallel momenta up to the zone edge and even beyond. The computed values of β and Q_c for LiF and KCN are somewhat large compared with the corresponding values obtained for metals. For metals the typical values are in the range $\beta \approx 2$ Å^{-1} and $Q_c \approx 1$ Å^{-1} [10]. In the case of LiF and KCN, the large values estimated for β indicate much stiffer potentials. Similarly, the large Q_c values obtained (which facilitate scattering to larger parallel momenta) are consistent with the highly corrugated and rough nature of the surfaces of these materials.

Acknowledgements

The experimental data used in our analysis were provided by Jeff Baker and Greg Bishop of the Helium Scattering Studies group at Florida State University, headed by Profs. J.G. Skofronick and S.A. Safron. Their cooperation is highly appreciated. This research is supported by NSF grant No. DMR 9114015.

References

[1] V. Bortolani and A.C. Levi, Rivista del Nuovo Cimento 9 (1986) 1.
[2] J.P. Toennies, Phys. Scripta T 19 (1987) 39.
[3] J.R. Manson, Phys. Rev. B 43 (1991) 6924.
[4] J.R. Manson, Comput. Phys. Commun. 80 (1994) 145.
[5] J. Böheim and W. Brenig, Z. Phys. B 41 (1983) 243.
[6] K. Burke, B. Gumhalter and D.C. Langreth, Phys. Rev. B 47 (1993-I) 12852.
[7] R. Brako and D.M. Newns, Phys. Rev. Lett. 48 (1982) 1859; Surf. Sci. 123 (1982) 439.
[8] R. Brako and D.M. Newns, Surf. Sci. 123 (1982) 439.
[9] N.W. Ashcroft and N.D. Mermin, Solid State Physics (Saunders, New York, 1976).
[10] F. Hofmann, J.P. Toennies and J.R. Manson, J. Chem. Phys. to be published.
[11] V. Celli, in Many Body Phenomena at Surfaces, eds. D. Langreth and H. Suhl (Academic Press, New York, 1984) p. 315.
[12] V. Celli, G. Benedek, U. Harten, J.P. Toennies, R.B. Doak and V. Bortolani, Surf. Sci. 143 (1984) L376.
[13] F.O. Goodman and H.Y. Wachman, Dynamics of Gas–Surface Scattering (Academic Press, New York, 1976).
[14] S.M. Weera and J.R. Manson, J. Electron. Spectrosc. 64/65 (1993) 707.
[15] J.M. Rowe, J.J. Rush, N.J. Chesser, K.H. Michel and J. Naudts, Phys. Rev. Lett. 40 (1978) 455.